Citation :
Rexer M, Hirt C (2015) Ultra-high Degree Surface Spherical Harmonic Analysis using the Gauss-Legendre and the Driscoll/Healy Quadrature Theorem and Application to Planetary Topography Models of Earth, Mars and Moon, *Surveys in Geophysics*, 36(6), pp 803-830, DOI: 10.1007/s10712-015-9345-z, Springer Netherlands

Ultra-high degree surface spherical harmonic analysis using the Gauss-Legendre and the Driscoll/Healy quadrature theorem and application to planetary topography models of Earth, Mars and Moon

Moritz Rexer[1] · **Christian Hirt**[2,1]

Submitted: July 2015 / Accepted: October 2015

Abstract In geodesy and geophysics, spherical-harmonic techniques are popular for modelling topography and potential fields with ever-increasing spatial resolution. For ultra-high degree spherical harmonic modelling, i.e. degree 10000 or more, classical algorithms need to be extended to avoid under- or overflow problems associated with the computation of Associated Legendre Functions (ALFs). In this work two quadrature algorithms - the Gauss-Legendre (GL) quadrature and the quadrature following Driscoll/Healy (DH) - and their implementation for the purpose of ultra-high (surface) spherical harmonic analysis of spheroid functions are reviewed and modified for application to ultra-high degree. We extend the implementation of the algorithms in the SHTOOLS software package (v2.8) by 1) the X-number (or Extended Range Arithmetic) method for accurate computation of ALFs and 2) OpenMP directives enabling parallel processing within the analysis. Our modifications are shown to achieve feasible computation times and a very high precision: a degree-21600 band-limited (=frequency limited) spheroid topographic function may be harmonically analyzed with a maximum space-domain error of 3 x 10^{-5} m and 5 x 10^{-5} m in 6 h and 17 h time using 14 CPUs for the GL and for the DH quadrature, respectively. While not being inferior in terms of precision, the GL quadrature outperforms the DH algorithm in terms of computation time. In the second part of the paper, we apply the modified quadrature algorithm to represent - for the first - time gridded topography models for Earth, Moon and Mars as ultra-high degree series expansions comprising more than 2 billion coefficients. For the Earth's topography, we achieve a resolution of harmonic degree 43,200 (equivalent to ~ 500 m in the space domain), for the Moon of degree 46,080 (equivalent to ~ 120 m) and Mars to degree 23,040 (equivalent to ~ 460 m). For the quality of the representation of the topographic functions in spherical harmonics we use the residual space domain error as an indicator, reaching a standard deviation of 3.1 m for Earth, 1.9 m for Mars and 0.9 m for Moon. Analysing the precision of the quadrature for the chosen expansion degrees, we demonstrate limitations in the implementation of the algorithms related to the determination of the zonal coefficients, which, however, do not exceed 3 mm, 0.03 mm and 1 mm in case of Earth, Mars and Moon, respectively. We investigate and interpret the planetary topography

[1] Institute for Astronomical and Physical Geodesy · Institute for Advanced Study, Technische Universität München
Arcisstrasse 21, D-80333 München
Tel.: +49-(0)89-289-23190
Fax: +49-(0)89-289-23178
E-mail: m.rexer@tum.de

[2] The Institute for Geophysical Research · Western Australian Geodesy Group · Department of Spatial Sciences, Curtin University of Technology
GPO Box U1987, Perth, WA 6845
Tel.: +49 (0)89-289-23198
Fax: +49-(0)89-289-23178
E-mail: c.hirt@tum.de

spectra in a comparative manner. Our analysis reveals a disparity between the topographic power of Earth's bathymetry and continental topography, shows the limited resolution of altimetry-derived depth (Earth) and topography (Moon, Mars) data and detects artifacts in the SRTM15 PLUS data set. As such, ultra-high degree spherical harmonic modeling is directly beneficial for global inspection of topography and other functions given on a sphere. As a general conclusion, our study shows that ultra-high degree spherical harmonic modeling to degree $\sim 46,000$ has become possible with adequate accuracy and acceptable computation time. Our software modifications will be freely distributed to fill a current availability gap in ultra-high degree analysis software.

Keywords Spherical Harmonic Analysis · Quadrature · Gauss-Legendre · Driscoll/Healy · Topography · Digital Elevation Model · Earth · Mars · Moon

1 INTRODUCTION

1.1 Motivation

The application of spherical harmonic modeling has a long tradition in Earth and planetary sciences such as geodesy and geophysics (see e.g. Sneeuw (1994), Wieczorek (2007), Balmino et al (2012), Wieczorek (2015)). The representation of a function (e.g. gravity field functionals, topography, magnetic field strength, etc.) on a spheroid planet in spherical harmonics (SH) can be used to (1) explore the spectral constituents of a global function (e.g. through global power spectral densities), (2) spherical harmonic modeling (e.g. combination of satellite data and/with terrestrial data (Pail et al, 2011)), (3) enable transforms in the spectral domain (e.g. spectral forward modeling of the topographic potential (Claessens and Hirt, 2013)) or (4) to interpolate between discrete points. The two mathematical processes to expand a function in the spatial domain into spherical harmonics, i.e. spherical harmonic coefficients (SHCs), and vice versa are known as the spherical harmonic analysis (SHA) and the spherical harmonic synthesis (SHS), respectively.
Today, many space-borne observation techniques are delivering high-resolution global data sets (i.e. ten metres to a few hundreds of metres in terms of global topographic data sets : TanDEM-X (Bartusch et al, 2008) surveyed the Earth with 12 m resolution, LOLA (Smith et al, 2010) surveyed the Moon with up to 30 m resolution). Further, there is an environmentally- and politically-driven growing demand for geophysical and environmental modeling. In consequence, the requirements for spherical harmonic computations concerning (1) spatial resolution, (2) numerical accuracy and (3) computational aspects such as memory and computation times steadily increase. For ultra-high degree (i.e. spherical harmonic degrees of 10,800 and beyond) spherical harmonic synthesis, free software has become available with the Matlab-based Graflab by Bucha and Janák (2013). However, as far as the ultra-high degree SHA is concerned, there is demand to review the existing SHA methods, eventually providing suitable SHA algorithms and software with ultra-high degree capability to the scientific community.

1.2 Past work

The Fast Fourier Technique (FFT) (Walker, 1996) for spherical harmonic analysis is a method of choice as it allows efficient evaluation of integrals in the frequency domain (with transformations between spatial and frequency domain). The most important prerequisite for the FFT is that the data is sampled on a regularly arranged grid. In general, a spherical harmonic analysis using FFT can be performed by numerical integration (=quadrature) following certain sampling theorems or by Least-Squares (LSQ) techniques (Sneeuw, 1994). The advantage of the latter is that it is the only SHA technique that allows stochastic modeling and hence is capable of delivering variance-covariance information for the estimated spherical harmonic parameters. The major drawback of the LSQ technique is that for ultra-high spherical harmonic degrees the normal equations become extremely large and require large-scale computational resources for its inversion (see e.g. Fecher et al (2013)). In comparison, quadrature techniques are more efficient to handle, as they usually (only) require a number Fast Fourier Transforms and series expansions (see also 2.1).

The theoretical foundations and derivations of quadrature techniques for SHA are well known. For a sound overview on most common methods and related literature see Sneeuw (1994), Claessens (2006), Driscoll and Healy (1994)). Few work exists on the implementation of ultra-high resolution spherical harmonic analysis techniques. Recently, some works were published that comprise spherical harmonic computations up to degree 10,800 at maximum (Gruber et al, 2011; Abrykosov et al, 2012; Balmino et al, 2012), which is the lower limit of the degree range taken into consideration in this work.

In Balmino et al (2012) 1 arc-min topography is analysed "by a standard quadrature method applied to $1' \times 1'$ equiangular mean values, and accelerated by the Longitude Recursion-Partial Sums algorithm". Numerical stability of the computed integrals of Associated Legendre Functions (ALFs) above degree and order (d/o) 2700 is achieved by the authors by multiple application of a normalization factor which prevents overflow with respect to the IEEE limitations on real numbers (Balmino et al, 2012). Abrykosov et al (2012) analyse a 1 arc-min gravity anomaly grid. The work relies on the 2D-FFT method by Gruber et al (2014) that circumvents shifts of the FFT base by latitude dependent phase lags, which occur when data is given in geodetic latitudes and cannot be treated efficiently by an FFT algorithm. The computation of ALFs in Gruber et al (2011, 2014) is based on Fourier expansions of associated Legendre functions (Hofsommer and Potters, 1960), modified as described in Gruber (2011).

The cited works and this work deal with the harmonic transformation based on spherical harmonic base-functions. With respect to the rotationally flatness of most planets, the use of ellipsoidal harmonics (EH) is possible likewise (see e.g. Dassios (2012)). EH may even seem more natural, however, ellipsoidal harmonic tools are not (yet) widely used.

1.3 This work

This paper primarily deals with the computational realization and validation of two numerical quadrature techniques for ultra-high resolution (surface) spherical harmonic analysis ($\geq$ degree 10,800): the Gauss-Legendre quadrature and the quadrature based on Driscoll/Healy's sampling theorem. As a second aspect we exemplify the application of the methods to ultra-high resolution planetary topography. We make use of the implementation of both techniques in the Fortran (F90)-based SHTOOLS v2.8 package (`http://SHTOOLS.ipgp.fr/`) written by Mark Wieczorek. The relevant routines are extended here with (1) stable algorithms for the computation of the fully-normalized Associated Legendre Functions based on the extended range arithmetic approach (Fukushima, 2012) and (2) parallel processing using OpenMP standards. First, the newly derived routines are validated in a closed loop environment of consecutive analysis and synthesis up to spherical harmonic degree 21600 (later during application the routines are validated indirectly up to degree 46080). Then the routines are used to investigate the characteristics and differences in spectral energy of the planetary topography of Earth and Mars as well as the Moon's body up to ultra-fine scales based on SRTM15 PLUS and the available PDS (Planetary Data System) data sets. Major motivation for the analysis of the high-resolution topography is that surface spherical harmonic coefficients of different powers of the topography may be used to forward-model the gravitational potential in the spectral (i.e. the spherical harmonic) domain (see e.g. Rummel et al (1988); Wieczorek (2007); Balmino et al (2012); Claessens and Hirt (2013); Hirt and Kuhn (2014)) at scales far beyond the resolution of gravity-capturing satellite missions such as the *Gravity and steady-state Ocean Circulation Explorer* (GOCE) (ESA, 1999), for Earth, or the *Gravity Recovery and Interior Laboratory* (Grail) (Lemoine et al, 2014), for the Moon.

The paper is outlined as follows: Section 2 briefly introduces the spherical harmonic series expansion and recapitulates the basic theory of numerical quadrature. In section 3 the modifications for making the previously introduced algorithms suitable for ultra-high degree SHA by extending the SHTOOLS package is described. Computation times, allocated memory and precision of the algorithms is discussed in section 3.2 and 3.3. In section 4 the procedures are applied to planetary topography models of Earth, Mars and Moon (section 4.1), revealing their spectrum up to degree and order 43200, 23040 and 46080, respectively. The application of our procedures is described in section 4.2,

and the results and the overall performance are discussed in section 4.3 and 4.4, respectively. Finally, we summarize the main findings of this work and give an outlook on future work in section 5.

2 THEORY

2.1 Spherical Harmonic Analysis by Quadrature

Quadratures here denote methods that translate a function on a spheroid into its spectral constituents w.r.t. the spherical harmonic base-functions by means of numerical integration. It is thus, in a more general view, a spherical harmonic analysis procedure such as SHA based on least-squares (Sneeuw, 1994) or collocation techniques (Moritz, 1978; Arabelos and Tscherning, 1998). Sneeuw (1994) showed that an approximate quadrature can be derived from the least-squares collocation formulation. For fundamental mathematical relations concerning spherical harmonic analysis see e.g., Hofsommer (1957); Colombo (1981) and Sneeuw (1994).
Following the explanations in Sneeuw (1994), in continuous space the harmonic coefficients C_{nm} and S_{nm} may be defined by the two integrals

$$\left\{ \begin{array}{c} A_m(\theta) \\ B_m(\theta) \end{array} \right\} = \frac{1}{(1+\delta_{m0})\pi} \int_0^{2\pi} f(\theta,\lambda) \left\{ \begin{array}{c} \cos m\lambda \\ \sin m\lambda \end{array} \right\} \partial\lambda \tag{1}$$

$$\left\{ \begin{array}{c} \bar{C}_{nm} \\ \bar{S}_{nm} \end{array} \right\} = \frac{1+\delta_{m0}}{4} \int_0^{\pi} \bar{P}_{nm}(\cos\theta) \left\{ \begin{array}{c} A_m(\theta) \\ B_m(\theta) \end{array} \right\} \sin\theta\partial\theta \tag{2}$$

where f is the function on a sphere with spherical coordinates θ (co-latitude) and λ (longitude), $\bar{P}_{nm}$ are the fully-normalized associated Legendre functions of the first kind with

$$\delta_{m0} = \left\{ \begin{array}{ll} 1, & m = 0, \\ 0, & m \neq 0. \end{array} \right\}. \tag{3}$$

The spherical harmonic degree and order are *n* and *m*, respectively, while $\partial\lambda$ and $\sin\theta\partial\theta$ are the differentials indicating the integration variables.
Eq. 1 and Eq. 2 can directly be translated into discrete space, giving the basic formulas for an approximate quadrature (here modified after Sneeuw (1994))

$$\left\{ \begin{array}{c} A_m(\theta_i) \\ B_m(\theta_i) \end{array} \right\} = s_i \; \frac{1}{N\;(1+\delta_{m0}+\delta_{mL})} \sum_{j=0}^{2N-1} f(\theta_i,\lambda_j) \left\{ \begin{array}{c} \cos m\lambda_j \\ \sin m\lambda_j \end{array} \right\} \tag{4}$$

$$\left\{ \begin{array}{c} \bar{C}_{nm} \\ \bar{S}_{nm} \end{array} \right\} = \frac{1+\delta_{m0}}{4} \sum_{i=1}^{N} \bar{P}_{nm}(\cos\theta_i) \left\{ \begin{array}{c} A_m(\theta_i) \\ B_m(\theta_i) \end{array} \right\} \tag{5}$$

where N denotes the number of latitude parallels (the equation holds for an equiangular grid, with $2N-1$ meridian parallels) and s_i is a weight which is proportional to the sine of the co-latitude (akin to the $sin\theta d\theta$ term in Eq.2). The weights may be seen as a means to account for the meridian-convergence-implied distortion of the scaling in each latitude parallel.

2.1.1 Approximate quadrature

According to Sneeuw (1994) the weights s_i may be chosen as

$$s_i = \frac{\pi}{N} \sin\theta_i, \tag{6}$$

or

$$s_i = \frac{2}{\sum_{k=1}^{N} \sin\theta_k} \sin\theta_i \tag{7}$$

and, inserted into Eq.5 and Eq. 4, may be used as formula for an approximate quadrature. However, the weights in Eq. 6 and 7 do not account for the fact that some of the base functions, namely

the Legendre functions, loose their orthogonality in the discrete case (Sneeuw, 1994), and thus, applied in the quadrature, yield approximate values for the harmonic coefficients only. Two (known) possibilities to ensure the orthogonality of the discretised Legendre functions by certain weighting and sampling schemes are presented in section 2.1.2 and 2.1.3, leading to an exact harmonic retrieval of spherical functions by numerical integration.

2.1.2 Exact quadrature through Driscoll/Healy

Following the quadrature based on Driscoll and Healy's (DH) algorithm (Driscoll and Healy, 1994), the geographic data has to be provided on a regular (quadratic) grid of $[2n_{max}+2 \times 2n_{max}+2] = [N \times N]$ grid points, where n_{max} is the maximum spherical harmonic degree (and order) of the coefficients. with latitude parallel sampling of $\Delta\theta = 180°/N$ and meridian sampling of $\Delta\lambda = 360°/N$ or on a larger (truly) equiangular grid ($[N \times 2N]$) with $\Delta\theta = \Delta\lambda = 180°/N$. The additional information in the larger grid is ignored by the algorithm, however, grids dimensioned with $N \times 2N$ are often used by global geographic data sets and therefore might be the more practicable grid size. The number of samples, N, must be even for this type of quadrature and the spherical harmonic expansion is exact if the function represented by the grid is band-limited to degree $n_{max} = N/2 - 1$. More precisely, the algorithm is based on the fact that „a function, whose Fourier transform has bounded support, may be recovered "from its uniformly arranged samples „with a frequency a least twice the bounding frequency "(Driscoll and Healy, 1994).
To account for the fact that the sample points near the poles are closer to each other than they are near the equator, latitude-dependent sample weights are introduced (Driscoll and Healy, 1994), achieving orthogonality of the base functions. The weights a_i are given in Driscoll and Healy (1994) (eq. 9, p. 216) as

$$a_i = 4\pi \frac{2\sqrt{2}}{N} \sin\left(\frac{\pi i}{N}\right) \sum_{l=0}^{N/2} \frac{1}{2l+1} \sin\left((2l+1)\frac{\pi i}{N}\right) \quad for\ i = 0, ..., N-1 \tag{8}$$

where the factor 4π additionally is introduced into the original equation, as Driscoll and Healy (1994) use unity normalized spherical harmonics and the quadrature is based on 4π - normalised spherical harmonics (as is common in geodesy). Then the coefficients A_m and B_m within Driscoll and Healy's method for an equiangular grid become

$$\begin{Bmatrix} A_m(\theta_i) \\ B_m(\theta_i) \end{Bmatrix} = \frac{\sqrt{2}}{\pi} a_i \sum_{j=0}^{2N-1} f(\theta_i, \lambda_j) \begin{Bmatrix} \cos m\lambda_j \\ \sin m\lambda_j \end{Bmatrix} = \frac{\sqrt{2}}{\pi} a_i \begin{Bmatrix} Re\left(F_m\left(f\left(\theta_i, \lambda_1 ... \lambda_{2N-1}\right)\right)\right) \\ -Im\left(F_m\left(f\left(\theta_i, \lambda_1 ... \lambda_{2N-1}\right)\right)\right) \end{Bmatrix} \tag{9}$$

and with Eq. 9 inserted into Eq. 5 the surface spherical harmonic coefficients my be retrieved. The variable F_m denotes the complex valued Fast Fourier Transform which is computed for each i^{th} latitude parallel of the gridded functional $f(\theta_i, \lambda_i ... \lambda_{2N-1})$ and contains the Fourier coefficients (real (Re) and imaginary (Im) part of F_m). The back- and forward Fourier transformations are possible because of the periodicity of the function described by each latitude parallel and because of the orthogonality of the sine and cosine functions (c.f. Sneeuw 1994).
Note that due to the oversampling needed for the algorithm N or $2N$ complex Fourier coefficients are computed (for a quadratic or an equiangular grid, respectively) for each parallel, of which only $\frac{N}{2} - 1$ ($= n_{max} = m_{max}$) are used. All frequencies $n > \frac{N}{2} - 1$ are simply discarded as they would lead to aliasing.

2.1.3 Exact quadrature through Gauss-Legendre

Following the Gauss-Legendre-Quadrature (GLQ) (or *second Neumann method* in Sneeuw (1994)), an irregular grid ($[n_{max}+1 \times 2n_{max}+1] = [N \times 2N-1]$) with equidistant sampling along latitude parallels and variable sampling along meridians is established. On the meridians grid points are at the zero-crossings of the associated fully-normalized Legendre Polynomials, i.e. $\bar{P}_{n_{max}+1, m=0}(\cos\theta_i) := 0$. This grid is referred to as Gauss-Legendre grid or Gauss-Neumann grid

(Sneeuw, 1994).
Neumann's latitude dependent quadrature weights w_i (also called Legendre weights) ensure that the orthogonality of the discrete Legendre functions is guaranteed and are given, e.g. by Krylov (1962) in Sneeuw (1994)

$$w_i = \frac{2}{(1-\cos(\theta_i)^2)\left(P'_{n_{max}+1}(\theta_i)\right)^2} \qquad for\ i = 0, ..., N-1, \tag{10}$$

where $P^{'}$ is the first derivative of the Legendre Polynomial with respect to θ. Then the coefficients A_m and B_m within the GLQ become

$$\left\{ \begin{array}{c} A_m(\theta_i) \\ B_m(\theta_i) \end{array} \right\} = 2\ w_i \sum_{j=0}^{2N-1} f(\theta_i, \lambda_j) \left\{ \begin{array}{c} \cos m\lambda_j \\ \sin m\lambda_j \end{array} \right\} = 2\ w_i \left\{ \begin{array}{c} Re\left(F_m\left(f\left(\theta_i, \lambda_1 ... \lambda_{2N-1}\right)\right)\right) \\ -Im\left(F_m\left(f\left(\theta_i, \lambda_1 ... \lambda_{2N-1}\right)\right)\right) \end{array} \right\} \tag{11}$$

and with Eq. 11 inserted into Eq. 5 the surface spherical harmonic coefficients may be retrieved. The quadrature is exact when the function on the sphere is band-limited to degree $n_{max} = N - 1$.

3 COMPUTATIONAL ASPECTS

This section describes the implementation of the above algorithms for high degree SHA under computational and numerical aspects. Starting point for the realisation are existing (open-source) Fortran (F90) routines (`http://SHTOOLS.ipgp.fr/`) for both quadrature rules (DH and GLQ) in the SHTOOLS v2.8 package. The package written by Mark Wieczorek consists of a compilation of F90 routines dedicated to spherical harmonic computations (e.g. transformations, multitaper spectral analysis).
In SHTOOLS the implementation of the two quadrature algorithms given above by Eq. 9 and 11 inserted in Eq. 5 is done in a very efficient manner by (1) employing FFT for the evaluation of the sum over longitude-dependent cosine and sine arguments in each latitude parallel and by (2) exploiting the symmetry of the Legendre Polynomials and ALFs about the equator ($P_{nm}(\cos\theta) = P_{nm}(\cos -\theta)$). Due to the latter measure ALFs are computed only once for corresponding latitude parallels on the northern and southern hemisphere. In effect, the loop for the summation in Eq. 5 halves (upper summation index then is $N/2 + 1$), leading to significant acceleration of the quadratures. Additionally, the ALF computation is embedded in the routines, which is time-saving as multiple initializations are omitted and no calls to external modules/routines are necessary (see SHTOOLS routines: SHExpandDH.f90, SHExpandGLQ.f90).

3.1 Computation of ALFs

The key aspect facilitating numerically accurate spherical harmonic computations up to ultra-high degree and order is numerical stability in the evaluation of the fully normalised associated Legendre functions to ultra-high degree. In contrast to the fully-normalized associated Legendre Polynomials ($\bar{P}_{n0}$), the ALFs ($\bar{P}_{nm}$ with $m \neq 0$) are numerical inaccurate when evaluated with standard recursion formulas for high spherical harmonic degree and order. In the SHTOOLS package the computation of the associated Legendre functions is realized via the modified forward-column method (Holmes and Featherstone, 2002). This method is a modification of the standard forward column recursion which prevents over-/underflow of the ALFs (held in double precision variables) by applying a scaling factor of 1^{-280} at the beginning of the recursion. This modification allows the stable computation of Legendre Polynomials to degree 2700 (Holmes and Featherstone, 2002).
Aiming at higher degree computations, we incorporated the *Extended Range Arithmetic* (ERA) approach (Fukushima, 2012), also known as *Xnumber* approach, for the computation of fully normalised ALFs, instead. In theory, the ERA allows the stable evaluation of ALFs up to arbitrary degree and order. Within the algorithm under- overflow problems are omitted by extending the exponent of floating point numbers, keeping the numbers in the numerical range of ordinary double precision ($REAL^*8$) numbers. The ALF algorithms by Fukushima (2012) for the computation of the sectorial

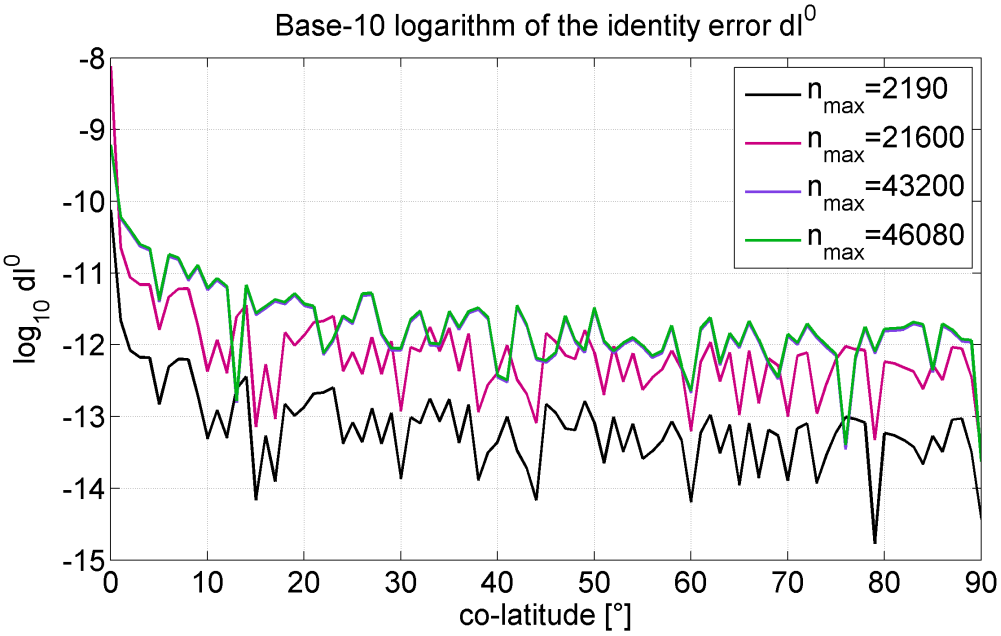

Fig. 1 Identity error I^0 (Eq. 13) of the implemented ALF algorithm for various maximum degrees per latitude parallel. Note that the green and blue curves are very close together.

and tesseral ALFs are complemented by a standard forward column method for the computation of the zonal Legendre Polynomials (which are unaffected by over-/underflow issues at ultra-high degrees). The zonal ($m = 0$) fully normalized Legendre Polynomials P_n follow the recursive description e.g. given in Holmes and Featherstone (2002) as

$$\begin{aligned} P_0 &= 1 \\ P_1 &= \sqrt{3}\sin\theta \\ P_n &= P_{n-1} \cdot \frac{\sqrt{(2n+1)(2n-1)}}{n} \cdot \cos\theta - P_{n-2} \cdot (n-1) \cdot \frac{\sqrt{2n+1}}{n \cdot \sqrt{2n-3}} \;, \; for\; n > 1. \end{aligned} \tag{12}$$

To verify the accuracy of the implemented ALF algorithm, tests with exact identities that represent certain sums of ALFs may be used (see e.g. identity tests provided in Holmes and Featherstone (2002); Fukushima (2012)). We use the identity error defined by

$$I^0 = \frac{\sum_{n=0}^{M} \sum_{m=0}^{n} P_{nm}(\cos\theta)^2}{(M+1)^2} - 1 \tag{13}$$

(c.f. Holmes and Featherstone (2002)), where the square-sum over all ALFs up to a certain maximum degree M for any θ in the interval $-90° < \theta < 90°$ must equal $(+1)^2$. Our tests (Fig. 1) show that for $M = 2190, 21600, 43200$ and 46080 the error stays well below 1^{-10} for $\theta > 5°$ and below 1^{-8} for polar latitudes ($\theta < 5°$). Note that for accurate computation of the identity error in Eq. 13 the variable holding the squared ALFs must be of quadruple precision (REAL*16).

We acknowledge other methods exist for the numerically stable computation of ALFs at ultra-high degree (see e.g., Balmino et al (2012) or Gruber (2011)), which could be considered for implementation too.

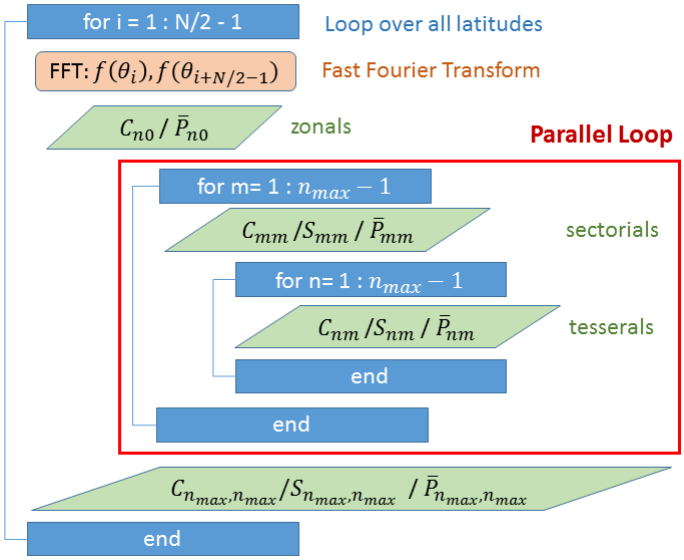

Fig. 2 Scheme of the general program structure of the SHTOOLS quadratures (applies for GLQ and DH) showing the location of the implemented OpenMP parallel loop directive in this work

3.2 Parallelisation and computation times

Ultra-high degree spherical harmonic computations require efficient parallel computation techniques. The reason is that the number of parameters and ALFs to be estimated or computed increases in quadratic manner with the maximum degree, by $(n_{max}+1)^2$. Simultaneously, the size of the grid increases quadratically, as raising the degree requires a finer sampling of the function to be analysed by the quadrature. An overview on the number of parameters, ALFs and grid points together with related memory allocation are given in table 1 for selected spherical harmonic degrees. A degree-21600 SHA thus requires the computation of 466.6 million spherical harmonic parameters and the same number of ALFs per latitude. Even when taking into account the symmetry of the ALFs to the equator a total of $\sim 10^{13}$ or $\sim 5 \cdot 10^{12}$ SHCs and ALFs need to be computed within the implementation of Driscoll/Healy's quadrature and the Gauss-Legendre quadrature, respectively. These large numbers already suggest that using a single CPU is hardly sufficient for high-degree quadratures. Therefore, we make use of the *OpenMP* Application Program Interface (API) (`www.openmp.org`), which provides a flexible interface for certain CPU directives, enabling shared-memory parallel programming for multiple platforms in C/C++ and Fortran.

In a first attempt we make use of the OpenMP *Parallel Loop* directive, which allows to share time-consuming loops among a predefined number of threads, i.e. CPUs. There are generally two major loops needed, one outer loop over all orders m and on inner loop over all degrees $n > m$, when it comes to the computation of all sectorial and tesseral SHCs associated to a certain latitude (and to its symmetrical counterpart) in Eq. 5 together with Eqs. 9 or 11. The parallel regions are embedded directly into the SHTOOL quadrature (and synthesis) routines (SHExpandGLQ.f95, SHExpandDH.f95, MakeGridGLQ.f95, MakeGridDH.f95) and embrace the computationally costly double loop (Fig. 2). Within the outer loop the ALF routine is called $n_{max}-1$-times to calculate a vector containing all ALFs of the same order m, which is then multiplied with the corresponding Fourier coefficients (or with the corresponding spherical harmonic coefficients in case of SHS routines) within the inner loop over all degree n for $n > m$. The resulting $(n_{max}-1)+(n_{max}-1)\cdot(n_{max})/2$ operations per latitude (e.g. ~ 233.3 million operations for $n_{max}=21600$) are shared between the allocated CPUs.

With this kind of parallel processing, computation times of the GLQ quadrature could be reduced approximately by a factor of 6 and by a factor of 13 of the time needed by a single CPU using 8 and 14 CPUs, respectively. In the case of using the DH algorithm in the quadrature, the parallelisation reduces to a fifth and a thirteenth of the time needed by a single CPU using 8 and 14

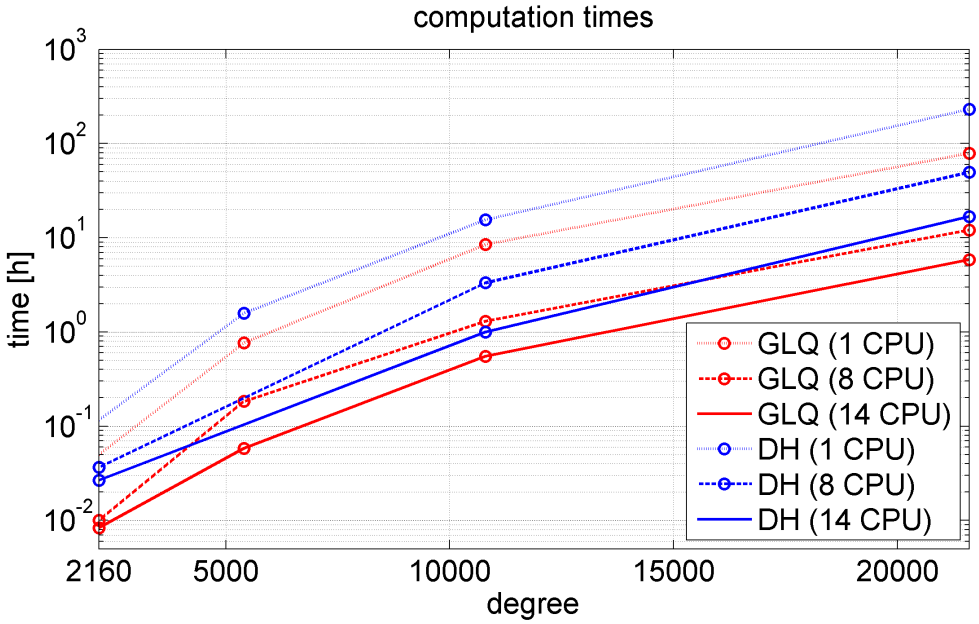

Fig. 3 Computation times for spherical harmonic analysis using the Gauss-Legendre quadrature (GLQ) and the Driscoll/Healy quadrature (DH) as a function of maximum recovered degree and allocated CPUs

CPUs, respectively. Absolute computation times of both algorithms are illustrated in Fig. 3. The *CPU time* (=computation time times number of used CPUs) of the here investigated SHA methods are significantly lower compared to e.g. the method suggested by Gruber et al (2011). A degree and order 10800 analysis in Gruber et al (2011) (c.f. table 1) takes ≈ 170 CPU hours (in a 16 thread environment), while it takes ≈ 8 CPU hours using the here implemented GLQ-quadrature (in a 14 thread environment).

We note that at degree 2160 the computation times are about 8 times longer compared to the original SHTOOLS quadrature routine which is based on the standard forward column recursion (47 seconds vs 376 seconds). The significant prolongation owes to 1) using the X-number routines for the computation of the ALFs, which are approximately a factor 2 more time consuming than the modified forward-column recursion (personal comm. Fukushima 2015), and to 2) calling an external routine for the computation of the X-number ALFs. In the original SHTOOLs implementation, the ALF computation is embedded in between the lines of the quadrature routine which means initialisation of parameters is only done once (and not m times) and storage of ALFs in large arrays is not required.

In a second attempt, we tried to assign a single core directly to the processing of a whole latitudinal parallel. This approach turned out to be not feasible because within each latitudinal parallel the CPUs have to update the array holding the SHCs. As the different CPUs may write (update) an allocated memory within the array at the same time, data integrity is not ensured. The OMP attribute clauses for shared variables, like ATOMIC or REDUCTION, would ensure this kind of integrity. Those attributes, however, only work for scalar variables. The variable holding the SHCs is an array of dimension $[2, n_{max}+1, n_{max}+1]$, and thus the attributes are not applicable here.

3.3 Precision of implemented algorithms

The implemented DH (section 2.1.2) and GLQ (section 2.1.3) quadratures are exact algorithms, only, when applied to a band/frequency-limited function that is discretised (or sampled) in the correct manner. In order to validate both algorithms we use band-limited variants of Earth's relief (topography and bathymetry), and perform two consecutive analysis and synthesis to create a closed loop experiment. First, DEM elevations are resampled according to the respective algorithms' sampling scheme (described above) by means of a 2D-interpolation (cubically). The obtained grids

n_{max}	SHCs number [mio]	SHCs memory* [GB]	Pnm/ALFs number [mio]	Pnm/ALFs memory^x [GB]	DH-Grid latitude parallels	DH-Grid points [mio]	DH-Grid memory [GB]	GLQ-Grid latitude parallels	GLQ-Grid points [mio]	GLQ-Grid memory [GB]
360	0.13	0.00	0.13	0.00	722	0.52	0.00	361	0.26	0.00
2160	4.67	0.04	4.67	0.04	4322	18.68	0.15	2161	9.34	0.07
5400	29.17	0.23	29.17	0.23	10802	116.68	0.93	5401	58.34	0.47
10800	116.66	0.93	116.66	0.93	21602	466.65	3.73	10801	233.31	1.87
21600	466.65	3.73	466.65	3.73	43202	1866.41	14.93	21601	933.18	7.47
43200	1866.33	14.93	1866.33	14.93	86402	7465.31	59.72	43201	3732.61	29.86
46080	2123.46	16.99	2123.46	16.99	92162	8483.83	67.95	47081	4246.87	33.97

Table 1 SHA parameter, array and grid sizes for various maximum spherical harmonic degrees n_{max}; DH - Driscoll/Healy ; GLQ - Gauss-Legendre-Quadrature; *: in SHTOOLS twice the memory denoted here is needed for the SHCs, as cosine- and sine-assigned SHCs are stored in separate arrays of size $(n_{max}+1)^2$; ^{x} : in SHTOOLS the Pnm/ALFs are computed on the fly for each latitude parallel, so a maximum number of n_{max} Pnm/ALFs need to be held at the same time.

n_{max}	Gauss-Legendre (GLQ)	Driscoll and Healy (DH)
$2,160$	3.09×10^{-9}	2.6×10^{-9}
$10,800$	2.10×10^{-6}	1.58×10^{-6}
$21,600$	2.63×10^{-5}	4.89×10^{-5}

Table 2 Maximum absolute space-domain error of closed loop experiments with band-limited variants of Earth's topography using the GLQ and the DH quadrature algorithm; units are in metres

are harmonically analysed via the implemented extended SHTOOLS quadratures. The computed spherical harmonic coefficients can then be used to create band-limited grids of DH or GLQ kind up to degree 21600, via another synthesis. The synthesis step is validated externally with the freely available GrafLab-Software (Bucha and Janák, 2013), a MATLAB-based synthesis for ultra-high spherical harmonic expansions. Our implementation of the synthesis based on SHTOOLS (see above) is in very good agreement with GrafLab, and errors in the space domain do not exceed $2\text{x}10^{-6}$ m at degree/order 21600.

The numerical precision of the quadratures given by the maximum absolute error of analysis and consecutive synthesis of the created band-limited topography function in the space domain is given in table 2 for selected maximum spherical harmonic degrees n_{max}. The maximum residual errors of both approaches (GL and DH) are in the same order of magnitude, not exceeding 5×10^{-5} m even at maximum degree 21600. This suggests that the implementation is well suited for ultra-high degree spherical harmonic analysis. Error patterns in the residuals are shown and discussed in section 4.4.1 and 4.4 up to maximum degree 46080.

4 APPLICATION TO PLANETARY TOPOGRAPHY

In this section the implementation of the GLQ quadrature (section 3) is applied to planetary topography of different resolution and features, followed by a discussion of computational aspects and interpretation of results.

4.1 Data

The two planets Earth and Mars as well as the Earth's Moon are found to be suited to extensively test the numerical quadrature algorithms described in section 2.1, mainly because high- resolution shape functions are available in public data sets, covering the bodies' surfaces in their entirety. Additionally, the bodies show very different characteristics and surface features at large, medium and small scales (Wieczorek, 2007). On Earth we have the clear and unique distinction between continents (topography) and oceans (bathymetry) along with plate margins accompanied by (active) rift, subduction and uplift zones. On Mars we find a unique dichotomy - an asymmetry between low elevations in the northern and high elevations in the southern hemisphere - as well as large impact basins, rifts and the monumental regional peaks of the Tharsis volcanoes near the equator. Next to the Tharsis volcanoes located is the highest peak known as Olympus Mons, reaching almost 22 km (Wieczorek, 2007). The Lunar topography, with its heavily cratered farside and comparatively smooth nearside (reasoned by the young basaltic material and the Moon's Earth-bound rotation), is home to the largest known impact structure in the solar-system: the giant South Pole-Aitken impact basin on the southern farside hemisphere with a total relief of over 10 km within a region of 2000 km diameter (Wieczorek, 2007). At the same time the central processes being responsible for the morphology are very different due to the very different outer conditions and forces present in the respective planetary system. Among others, the processes leading to unique surface structures are: exposure to solar radiation, existence and composition of atmosphere, tectonic and volcanic activity, existence of water and gravity.

Planetary topographic data sets are provided in terms of digital elevation models (DEMs) and have been used in spherical harmonic analyses in the past. To our knowledge the maximum degree of available SHCs does not exceed 10800 for Earth, 2600 for the Moon and 2600 for Mars. The

Planet	Degree	SHC Data Set	Reference	Topographic Data
Earth	10800	Earth2014	Hirt and Rexer (2015)	SRTM30plus v9, Bedmap2, SRTM v4.1, GBT v.3
Earth	10800	ETOPO1	Balmino et al (2012)	ETOPO1
Moon	2600	LOLA2600p	Wieczorek (2015)	LOLA
Mars	2600	MarsTopo2600	Wieczorek (2015)	MOLA

Table 3 Existing works on high-degree spherical harmonic analysis of planetary topography; SRTM: Shuttle Radar Topography Mission; GBT: Greenland Bedrock Topography; PDS: Planetary Data System; LOLA: Lunar Orbiter Laser Altimeter ; MOLA: Mars Orbiter Laser Altimeter;

corresponding data sets and references are listed in table 3.

Within the publicly provided data sets there generally exist limitations or inconsistencies which are independent of the provided data resolution. Those may e.g. be related to the technique of measurement and blur our knowledge about the surface elevations of a planet. On Earth, for example, we have large differences between the quality of topographic elevations and seafloor (=bathymetric) elevations. The first of which can be measured with various terrestrial/airborne/spaceborne sensors, while the latter is sensed directly only via local-scale ship soundings and determined globally indirectly via ties to the altimetric gravity field (Smith and Sandwell, 1994). According to Sandwell et al (2014) more than 50 % of the ocean is more than 10 km away from the next direct depth measurement. The highest resolution gravity field over the oceans is derived from satellite altimetry and available models reach $\sim 1'$ ($\cong 2$ km) resolution (Andersen et al, 2013; Sandwell et al, 2014) at best. However, the actual resolution in these models is dependent on the spacing (or density) and the orientation of the satellite altimeter ground-tracks. The available new altimeter data sets of CryoSat-2 and Jason-1 have a ground-track spacing of 2.5 km and 7.5 km (Sandwell et al, 2014), respectively. When combined with altimeter data of older satellites (Geosat and ERS-1) the gravity data can be used to retrieve seamounts between 1 and 2 km height (Sandwell et al, 2014). But due to the attenuation of the shorter wavelength gravity signals, the estimation of bathymetric heights from gravity works best in the wavelength-band from 12 km to 160 km (Sandwell et al, 2014), which means it is of lower quality at scales < 12 km. Further, the quality of the estimates decreases with the thickness of the seafloor (Sandwell et al, 2014).

On Mars and Moon the actual resolution also is dependent on the across-track spacing of the laser altimeters ground-tracks, and higher-resolution data products are released as soon as the measurement density is good enough that there are some samples per pixel accumulated (Neumann, 2010). However, the track density is lowest near the equator and highest towards the poles due to the (near) polar orbit. Owing to this fact, there exist gaps of up to 12 km between neighboring profiles at the equator in case of Mars. In the data products, these gaps are filled with interpolated values (Smith et al, 2003).

Further, deviations from the orbital inclination of 90° inherent to most orbiters leads to non or poor observations in polar regions (see (Farr et al, 2007) and (Tachikawa et al, 2011) for Earth or (Smith et al, 2003) for Mars) and can only partly be compensated by other missions or observation techniques.

4.1.1 Earth's Topography and Bathymetry

Earth's topography and bathymetry here is taken from the first version of the SRTM15 PLUS data set (`ftp://topex.ucsd.edu/pub/srtm15_plus/`). It is the 15 arc-second nominal resolution (~ 0.5 km) successor of the well-known 30 arc-second topography/bathymetry maps SRTM30 PLUS (Becker et al, 2009). SRTM15 PLUS contains a new combination of SRTM, ASTER and CryoSat-2 ice sheet data over land and is based on SRTM30 PLUS v11 over the oceans' bathymetry. The SRTM30 bathymetry was derived, in principle, from the anomalous gravity field as sensed by various satellite altimeters and was calibrated and augmented locally by ship sounding data aggregated over 40 years time (Smith and Sandwell, 1994). The bathymetric data in areas devoid ship-sounding has a resolution of ~ 12 km with a maximum resolution of 2 km, rather than the nominal 500 m resolution of SRTM15 PLUS (cf. Sandwell et al (2014), and Section 4.1). For more

details on the creation of the bathymetry and its accuracy the reader is referred to (Smith and Sandwell, 1994; Sandwell et al, 2014; Marks et al, 2010).
The elevations and depths are given in terms of orthometric heights (in metres) relative to the $EGM96$ geoid, which is referenced to the $WGS84$ ellipsoid and which in good approximation represents the mean sea level.

As the SRTM15 PLUS data refers to geodetic latitudes it has to be transformed to geocentric latitudes in order to be used by the quadratures correctly. This is done by a 2D- spline interpolation using the simple relation

$$tan\ \Theta = \frac{a^2}{b^2}\ tan\ \phi \tag{14}$$

(see, e.g., Torge (2001), p.95) between the spherical co-latitude Θ and the geodetic co-latitude ϕ, where a is the semi-major and b the semi-minor axis of the underlying ellipsoid, which is GRS80 (Moritz, 2000) in this case.
Further, we found $6,194,174$ NaN (not-a-number) flagged pixels in the SRTM15PLUS data set (0.17% of all pixels). We filled these data gaps with SRTM30PLUS information in order to get to a truly complete (=global) topography/bathymetry data set for Earth.

4.1.2 Martian Topography

The topography model for Mars originates from the Mars Orbiter Laser Altimeter (MOLA) which was part of the Mars Global Surveyor (MGS) mission. The MGS orbiter was operated between 1998 and 2006 in a near polar orbit (inclination $= 93^\circ$). We use the *Mission Experiment Gridded Data Record* (GDR) - digital topographic maps that are generated from the altimeter observation data accumulated over the entire primary mission - made available via NASA's *Planetary Data System* (PDS) (Smith et al, 2003). The maps are sampled at 128-pixel-per-degree (~ 460 m). The MOLA topography is referenced to an areoid, defining a surface of constant (gravitational and rotational) potential (12652804.7 m^2/s^2 as the mean value at the equator at an average radius of 3396.000 km) (Smith et al, 2003). The areoid may be calculated by the Goddard Mars Gravity Model GGM-2B (Lemoine et al, 2001) evaluated to degree and order 50 (Smith et al, 2003). The MOLA topography then is the difference between the real planetary radius and areoid at a certain planeteocentric longitude and latitude (IAU2000 coordinate system).
In case of Mars, the polar regions ($> +88^\circ$ and $< -88^\circ$ latitude) are not covered by the gridded data products of 128-pixel-per-degree due to the spatially limited availability of MOLA observations. Therefore we used the 64-pixel-per-degree elevation product in the polar regions instead, and oversampled it by means of a bi- cubical interpolation to reach a nominal global resolution of 128-pixel-per-degree.

4.1.3 Lunar Topography

The lunar topography originates from the Lunar Orbiter Laser Altimeter (LOLA) instrument of the Lunar Reconnaissance Orbiter (LRO) mission (Smith et al, 2010). The orbiter circulates the moon on a polar orbit since mid-2009. We use the NASA PDS *Gridded Data Record's* digital elevation model with 256-pixel-per-degree resolution (~ 120 m), provided in terms of an equidistant cylindrical map (Neumann, 2010). The elevations are referenced to a reference sphere of 1737.4 km radius. A planeto-potential topography, i.e. physically meaningful heights, similar to the Earth's and the Martian case could be derived for the Moon by subtracting a selenoid model from the planetary radius. The selenoid (=lunar geoid) can be derived from any potential model for the Moon.However, this is not required for the purpose of the present study.

4.2 Processing

For the spherical harmonic analysis of the planetary topography we choose the Gauss-Legendre quadrature as described and tested in section 2.1.3 and 3.2 . Both, the GLQ and the DH algorithm

Planet	Sampling			Harmonic	Topographic Data
	$[\frac{pixels}{degree}]$	[arc-sec]	[m]	degree	
Earth	240	15	~ 500	43200	SRTM15 PLUS v1
Mars	128	28.125	~ 460	23040	MOLA
Moon	256	14.0625	~ 120	46080	LOLA

Table 4 Spatial Resolution (sampling), maximum harmonic degree and sources of the data used in the spherical harmonic analysis of planetary topography (see also section 4.1) in this work; SRTM: Shuttle Radar Topography Mission; LOLA: Lunar Orbiter Laser Altimeter ; MOLA: Mars Orbiter Laser Altimeter;

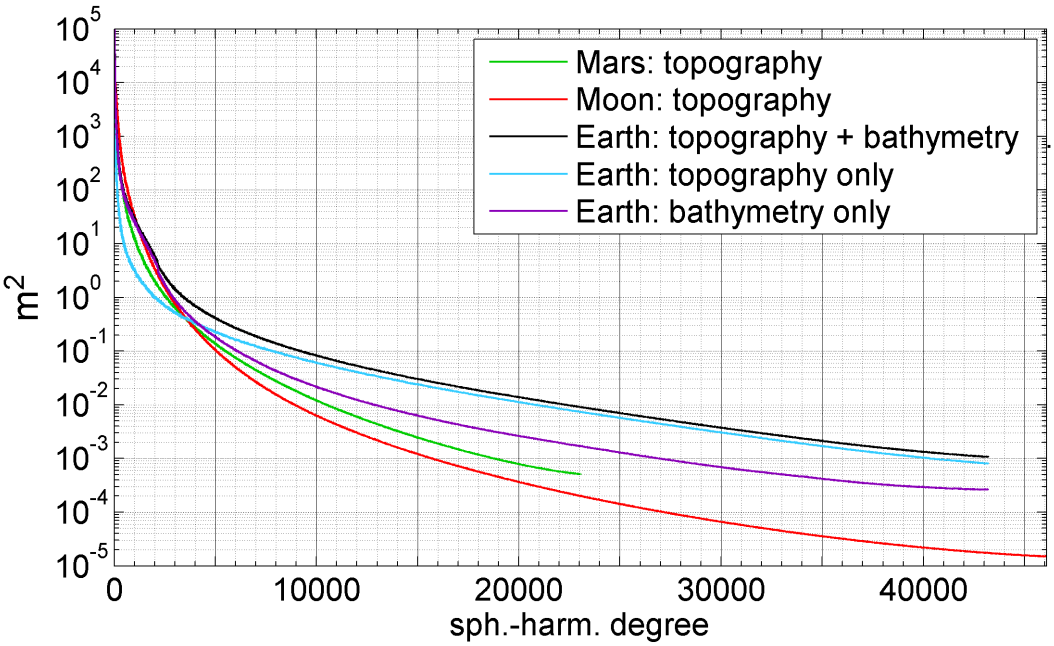

Fig. 4 Degree variances of planetary topography: Earth's topography and bathymetry in black, Earth's topography (ocean values set to zero) in light blue, Earth's bathymetry (continental values set to zero) in magenta, Lunar topography in red and the Martian topography in green; unit on y-axis is meters squared.

would be qualified for this task in terms of precision (see section 3.3), but because of comparatively long computation times the DH method is not efficient for ultra high degrees (> 10800), see section 3.2 and Fig. 3).

The spectral bandwidth of the real topography is unlimited, the recoverable spherical harmonic bandwidth of the topography, however, is limited by its discretisation(section 2.1). Thus the sampling of a discrete topographic function defines the degree of truncation in the spherical harmonic analysis (and leads associated truncation errors, see section 4.3). The sampling and the associated maximum recoverable degree of each topographic data set (section 4.1) are listed in table 4. In order to apply the Gauss-Legendre quadrature the latitude parallels have to coincide with the zero-crossings of the Legendre Polynomials (Eq. 12). This was achieved by bi-cubically interpolating topographic height values at the respective latitudes using Matlab's intrinsic 2D-interpolation method (cubic interpolater).

4.3 Results and discussion

The harmonic analysis reveals the spectral composition of Earth's topography and bathymetry to degree 43200 ($=500$ m half-wavelength), of the Martian topography to degree 23040 ($=460$ m half-wavelength) and of the Lunar topography to degree 46080 ($=120$ m half-wavelength). The degree

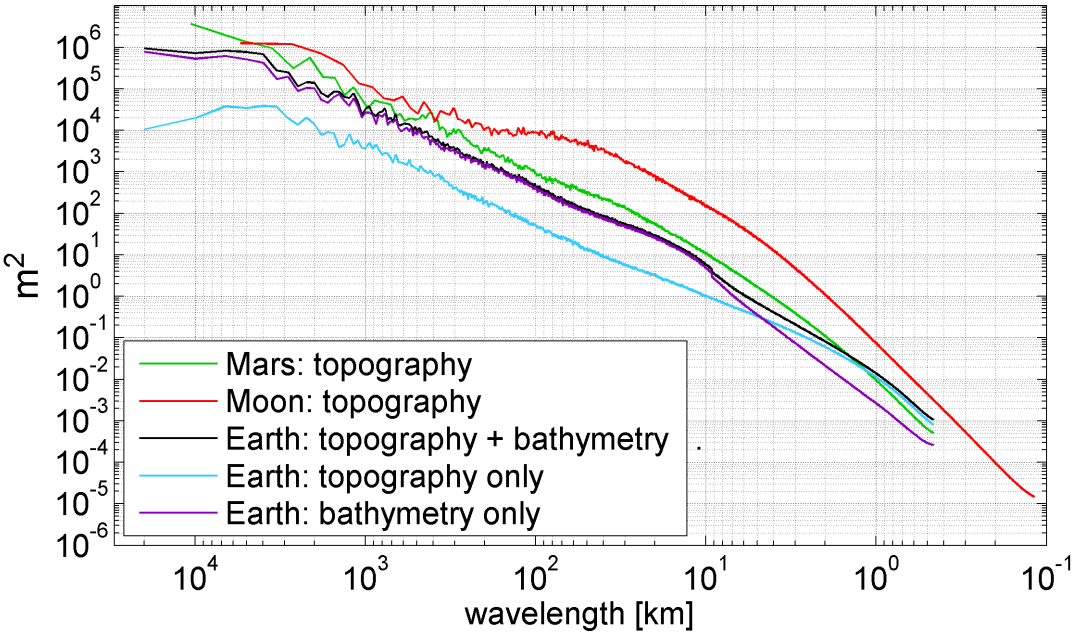

Fig. 5 Degree variances of planetary topography by associated spatial scale (half-wavelength in kilometres): Earth's topography and bathymetry in black, Earth's topography (ocean values set to zero) in light blue, Earth's bathymetry (continental values set to zero) in magenta, Lunar topography in red and Martian topography in green; unit on y-axis is meters squared.

variances are given in Fig. 4 and 5, as a function of harmonic degree and of the half-wavelength (=spatial resolution), respectively. At the same time re-expanding the calculated harmonic coefficients to a grid - sampled in the same manner as the input-grid - allows evaluation of the accuracy of the implemented GLQ quadrature for the different maximum degrees in a closed loop scenario (Fig. 6, 10, 12).

4.3.1 Spectra of planetary topography models

The topography of each planet exhibits different spectral energy towards ultra-short scales and the degree variances also reveal different decay of the topographic signal with harmonic degree (Fig. 4). Notably, it is Earth that has highest topographic energy beyond degree ~ 1900 (black curve), exceeding the Moon's topographic energy by almost 2 orders of magnitude at degree 43200. The major part of this short-scale energy is associated with Earth's continental topography. This can be seen from the harmonic analysis of the continental topography only (by setting all values below sea level to zero: light blue curve) and of the bathymetry only (by setting all values above sea level to zero: magenta curve). Bathymetry makes up most of the power in the black degree variance curve up to degree ~ 4000, whereas continental topography dominates Earth's spectral harmonic power beyond this degree. Adding the degree variances of the magenta and the light blue curve would lead to the full (topography and bathymetry) signal and result in the black curve (4).
The spectral properties of the martian and lunar topography are comparatively even (until degree 23040). The lunar degree variance curve (red) intersects with the martian curve (green) near degree 4000, having more power beyond this degree. Due to the limited grid resolution of the topographic data of Mars, only half of the spherical harmonic degrees could be recovered compared to the other two planets.
Translating the spherical harmonic degrees into spatial scales using each planet's natural half-wavelength (Fig. 5), allows to compare the spectral power in the degree variances of the different planets more intuitively, at the level of metric scales. Among the three bodies, the Moon's topography possesses the highest energy over all spatial scales, indicating that its planetary relief has a

higher variability (and thus roughness). Especially, at spatial scales of ~ 80 km to ~ 200 km there are several pronounced topographic features on the Moon (craters of similar size). This is to be seen in the degree variances of the lunar topography, which remain at the level of $\sim 10\text{x}10^4 m^2$, while the power of the other topography models (Earth and Mars) steadily decreases in this spectral band. In the lunar topography, this spectral bands represents several large-size Class 1 craters classified as TYC-type by (Wood and Anderson, 1978), e.g. Tycho (86 km diameter), Aristoteles (87 km diameter), Langrenus (132 km diameter) or Humboldt (207 km diameter). Those TYC craters are attributed multiple tiers of terraces, crenulated rim crest, large flat floor and a central peak (Wood and Anderson, 1978). Compared to Earth, also the Martian topography possesses more power at low and medium scales. Only below scales of 1.5 km the Martian topographic variability is below that of Earth's.

Compared with the topographic spectra of Moon and Mars, which show a very smooth decay (Fig. 4), the decay of Earth's topographic spectrum slows down in the band from ~ 30 km down to ~ 10 km (degree ~ 600 and 2160). Further, near degree 2160 a sudden drop in the power of the degree variances (see Fig. 4) or a change in tilt of the black curve (see Fig. 5), respectively, becomes visible. This behavior is attributable to the bathymetry component of the SRTM15PLUS model, which is seen from the inter-comparison of the three Earth power spectra (black vs. blue vs. magenta curve). We interpret the change of tilt at degree 2160 ($\sim 9-10$ km $\sim 4-5$ arc-minutes) to indicate the limit of the full resolution of bathymetric depth data (the seafloor mapping is not complete anymore at shorter spatial scales). This is supported by the assessment of the bathymetric resolution in section 4.1.

Note that the absolute power of the degree variances also depends on the sphere-aeroid and the sphere-geoid-separation, respectively, which has been treated differently for the planets or not at all in case of the Moon (see section 4.1). However, this effect is relevant only at long and medium spatial scales because the model- underlying geoid models are of rather smooth nature (maximum degree is 360 for SRTM30PLUS and 50 for MOLA).

4.3.2 Analysis of Earth's topography to d/o 43200

For Earth, the topography could be harmonically analysed to degree 43200. Using the computed SHCs for SHS, we can compare the resulting 15" x 15" grid with the SRTM15 PLUS input topography (Fig. 6: upper and middle plot). The standard deviation of the differences is about 1 m (RMS $=$ 3.06 m) in the space domain. Much of the differences (here further denoted as *residual error* but also found denoted as *representation error* by Balmino et al (2012)) occurs in high elevated or rough terrain (e.g. in the Himalayas with amplitudes of about ± 50 m, see middle plot in Fig. 7), whereas flat terrain (e.g. Australia) shows very small residual errors. Interestingly, apart from the mid-oceanic- ridges at the floor of the oceans, also linear residual error patterns become visible over the oceans. These linear errors seem to coincide with the ship routes that contributed the sounding data which was used to calibrate the SRTM15 PLUS bathymetry (Fig. 8). Obviously, these ship tracks create sharp edges in the modelled bathymetric surface. A much higher sampling frequency and higher degree in the analysis would be needed to be adequately represent those features in spherical harmonics. These residual errors together with the residual errors that appear in the areas of steep slopes (mountains, trenches) are here classified as truncation errors.

The minimum and maximum residual SHA/SHS error (-2447.31 m and 3498.47 m, respectively) is very high compared to the analysis of Mars and Moon (see further down). Importantly, they are the result of artifacts with sharp edges (or single pixel errors) detected in the SRTM15PLUS data set (Fig. 9) and are no sign for deficiencies in the quadrature algorithm.

4.3.3 Analysis of the Martian topography to d/o 23040

For Mars, the topography could be harmonically analysed to degree 23040 with a truncation error of about 0.4 m in terms of STD (RMS $=$ 1.94 m) in the space domain (Fig. 10: upper and middle plot). High residual errors are found around the highest elevated peaks (but not directly over the

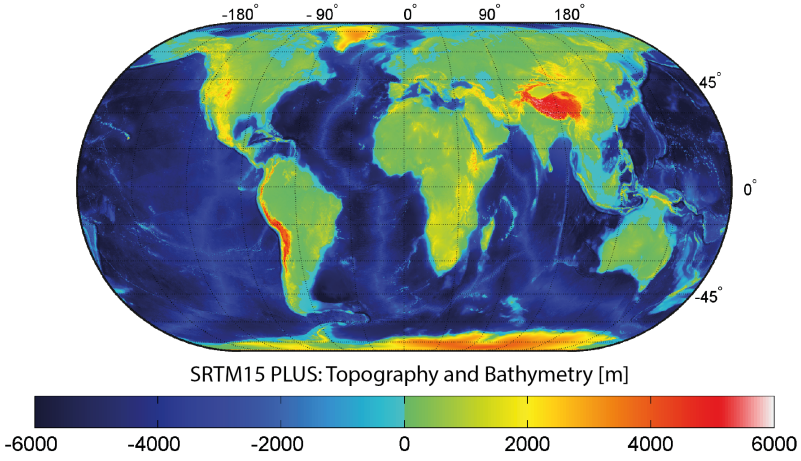

statistics [m]

min= -10930.10
max= 8681.24
rms= 3257,60
mean= -1888,67
std= 261,96

SHA/SHS retrieved grid:

min= -10931.65
max= 8658.67
rms= 3257,60
mean= -1888,67
std= 261,96

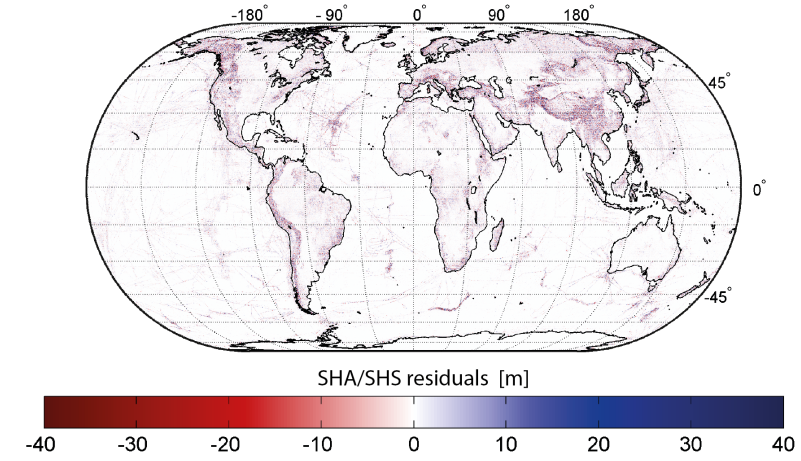

statistics [m]

min= -2447.31
max= 3498.47
rms= 3.06
mean= 0.00
std= 1.06

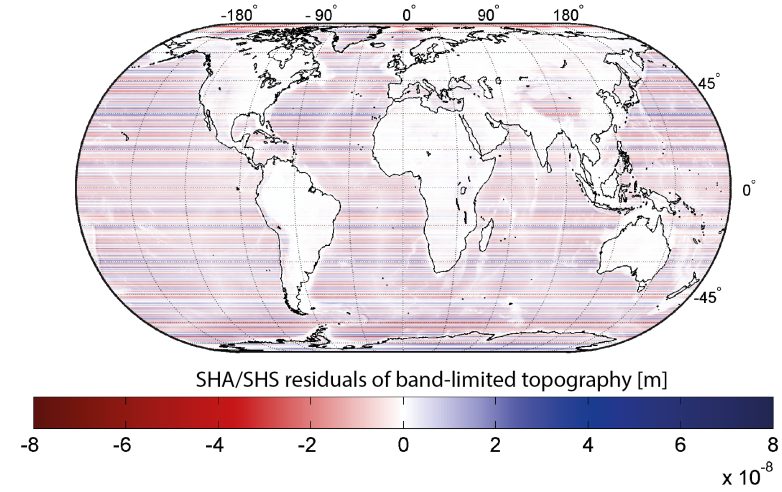

statistics [m]

min= -2.44e-03
max= 1.66e-03
rms= 1.40e-05
mean= -1.86e-08
std= 4.10e-08

Fig. 6 Earth's topography and bathymetry (upper plot), closed loop residuals with input topography after the first spherical harmonic analysis and synthesis (middle plot) and residuals of the anaylsis and synthesis of a band-limited input topography (to degree 43200); unit is metres.

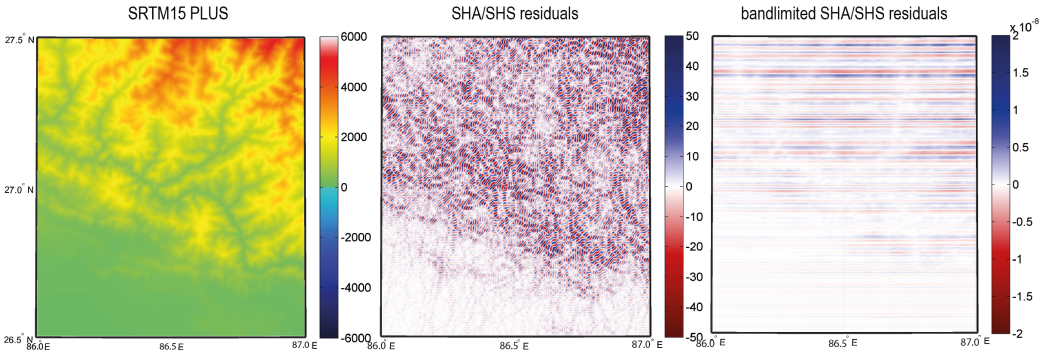

Fig. 7 Earth's topography (left plot), closed loop residuals with respect to input topography after the first spherical harmonic analysis and synthesis (middle plot) and residuals of the anaylsis and synthesis of a band-limited input topography (right plot) to degree 43200 over a selected region over the Himalayas; unit is metres.

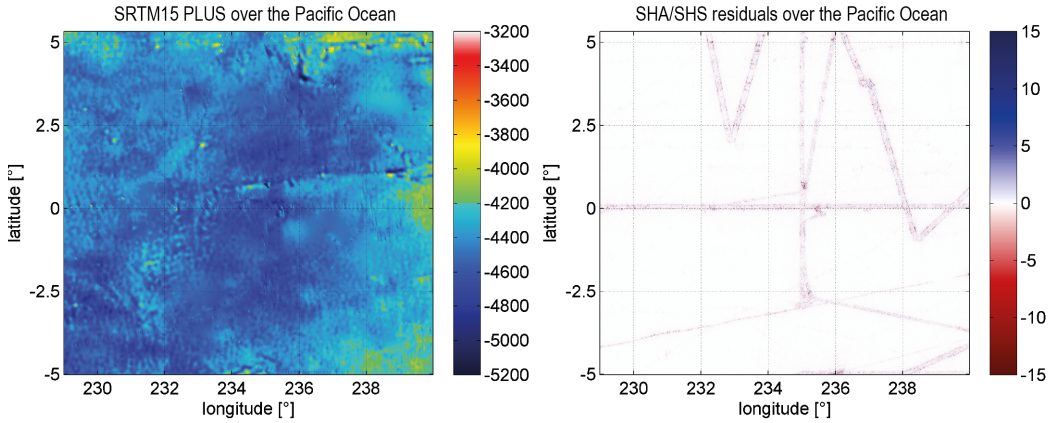

Fig. 8 Bathymetry over parts of the pacific ocean as contained in SRTM15PLUS (left) and the SHA/SHS residual error over this region (right), clearly depicting the ship- sounding tracks; unit is metres.

peaks), at the edges of some of the impact craters and along the deep rift valley such as the east-west aligned Vallis Marineris. The minimum and maximum errors are -1335.80 m and 937.75 m, respectively, less than in Earth's case.

Investigating different spectral bands of the MOLA topography by SHS, reveals a sightly inclined striping in the MOLA data (with $\sim 5-10$ m amplitude in the spectral band 17280...23040, Fig. 11). The stripes are also visible in the spectral band 11541...17279 (not shown here). Most probably the stripes are related to the ground tracks and ground coverage of the MOLA/MGS orbiter and illustrates the domain where MOLA DEM offers full resolution. Observation gaps existing between neighboring ground- tracks are filled by interpolation (Smith et al (2003) and see also section 4.1) and might thus be an explanation for the visible inconsistencies.

4.3.4 Analysis of the Lunar topography to d/o 46080

For Moon, the topography could be harmonically analysed to degree 46080 with a standard deviation of about 0.2m (RMS $= 0.91$ m) in the space domain (Fig. 12: upper and middle plot). The residuals on Moon show less co-location with topographic rough features (such as impact craters) and are generally of lower amplitude compared to those of the other planets analysed in this work. However, we find the amplitudes of the residuals slightly rising towards the poles.

By performing a synthesis in various spectral bands, we find certain bands affected by striping. In contrast to the striping in the MOLA data set, the stripes in LOLA data are north-south aligned and thus in along-track direction of the LRO spacecraft, that was navigated on a polar orbit. In the

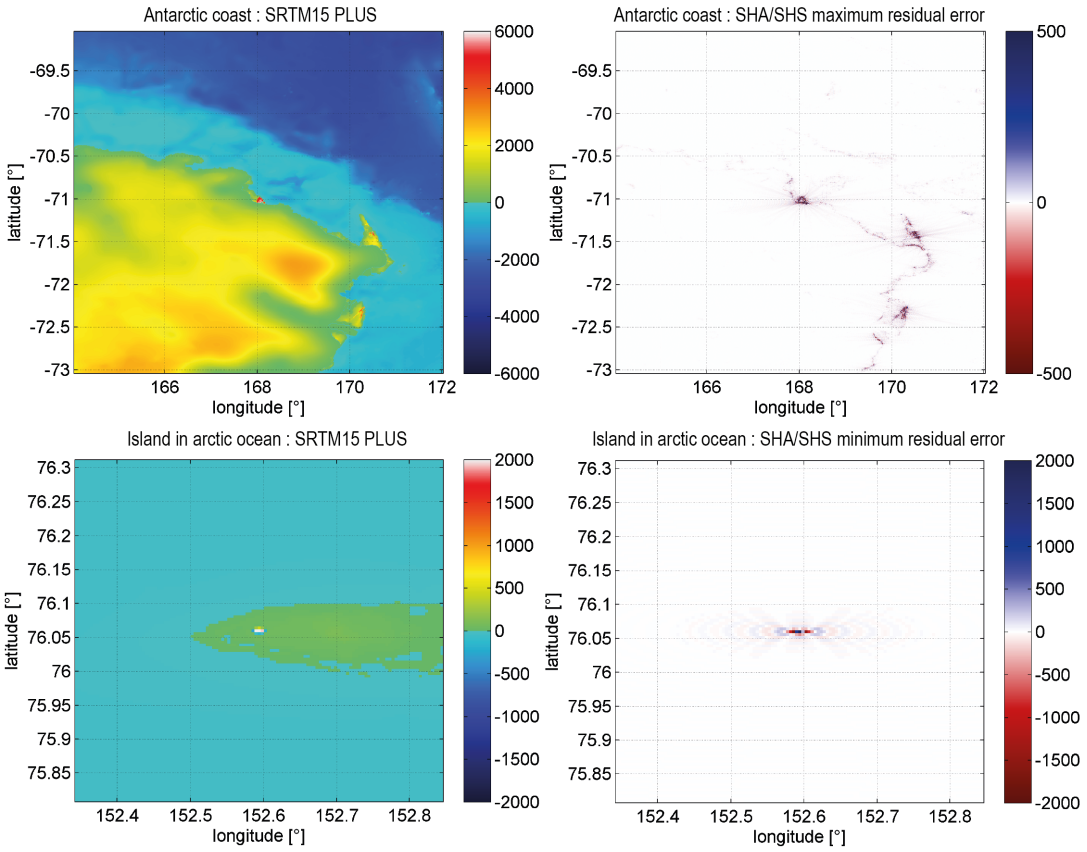

Fig. 9 Upper row: Area of minimum SHA/SHS residual error (-2447.31 m) in the SRTM15PLUS data set; Bottom row: Area of maximum SHA/SHS residual error (3498.47 m) in the SRTM15PLUS data set (note that some of the pixels on the island were NaNs and are filled by SRTM30PLUS values, see section 4.1.1); unit is metres.

band 23081...34620 the stripes have amplitudes at the $5-15$ m level (Fig. 13), indicating the limit in the resolution for the LOLA data.
MOLA/MGS has an inclined orbit and thus also the stripes are inclined against the north-south direction. We suspect the reason for LOLA and MOLA stripes to be of similar kind, and, to be related to the ground-track/ coverage of the laser altimeters.

4.4 Quadrature performance at ultra-high degrees

4.4.1 Accuracy and truncation errors of the analysis of planetary topography

The accuracy of the quadrature is not critically deteriorated by the choice of a higher spherical harmonic degree (see also section 3.3), as the Moon's much higher resolved topography is much better represented in spherical harmonics than Earth's topography. Instead, by interpreting the residuals (=differences to input topography shown in the middle plots of Fig. 6, 10 and 12) as truncation error, we learn that the choice of a higher harmonic degree in case of the Lunar topography (and the finer sampling intervals of the grid) leads to a lower truncation error (as expected). Taking the global topographic function's standard deviations as indicator for the overall roughness of a planet's topography, the Moon shows the highest variability (STD= 865.33 m), followed by Mars (STD=303.73 m) and Earth (STD= 261.96 m). Although Earth features the smoothest surface on average, it shows the highest truncation error.
Further we find that the accuracy of the quadrature locally is dependent on the topographic surface function itself, i.e. smoothness/roughness of the terrain, because the residuals coincide with the

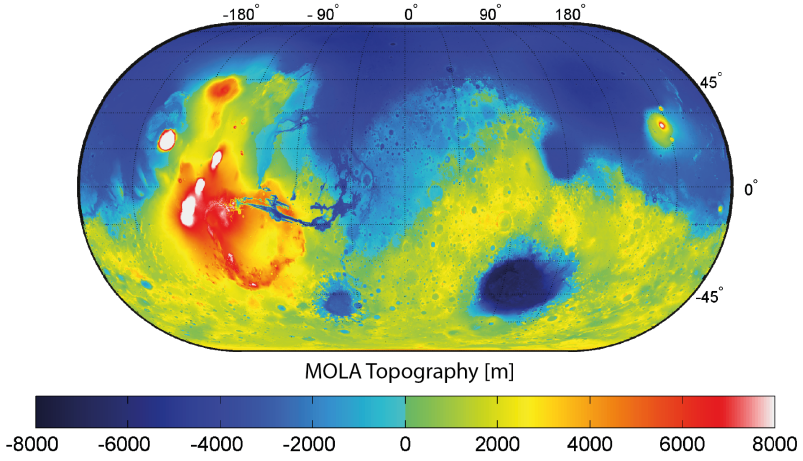

statistics [m]

min= -8202.37
max= 21277.74
rms= 3062.67
mean= -752.27
std= 303.73

SHA/SHS retrieved grid:

min= -8202.39
max= 21271.35
rms= 3062.67
mean= -752.27
std= 303.73

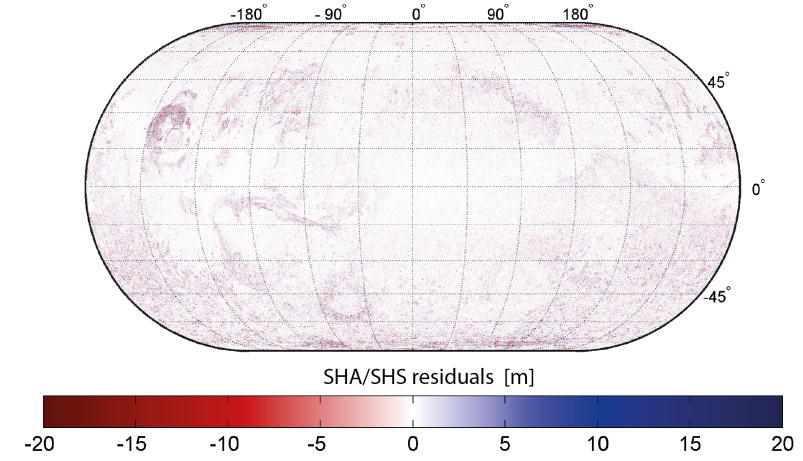

statistics [m]

min= -1335.80
max= 937.75
rms= 1.94
mean= 0.00
std= 0.44

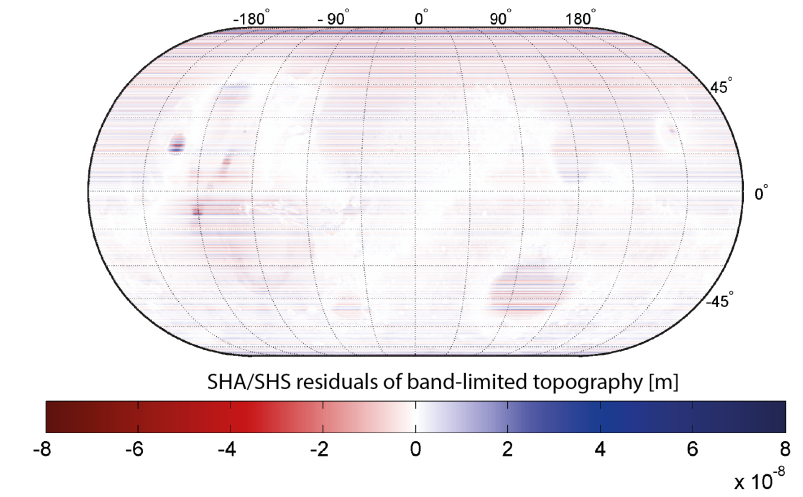

statistics [m]

min= -2.29e-05
max= 1.51e-05
rms= 2.21e-07
mean= -5.08e-10
std= 2.53e-10

Fig. 10 Martian topography (upper plot), closed loop residuals with input topography after the first spherical harmonic analysis and synthesis (middle plot) and residuals of the anaylsis and synthesis of a band-limited input topography (to degree 23040); unit is metres.

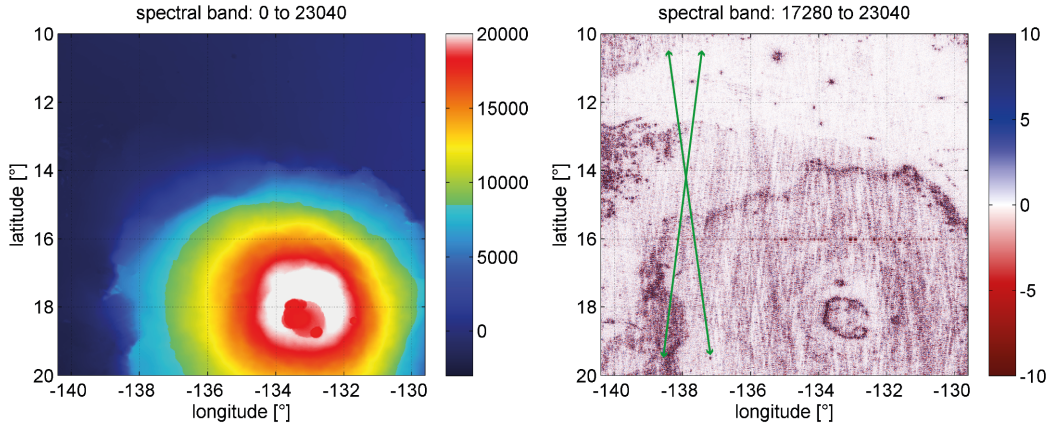

Fig. 11 Elevations around Olympus Mons obtained from a analysis and synthesis of MOLA data in the spectral band 0...23040 (left) and 17280...23040 (right); the green arrows indicate the direction of the visible striping pattern; unit is metres.

locations of mountains, steep slopes or edges (such as the ship sounding data tracks in Earth's bathymetry). This was also found by Balmino et al (2012).

4.4.2 Precision of the quadrature at ultra-high degrees

The residuals of each topographic input grid with respect to the topographic grid synthesized from its computed spherical harmonic coefficients reveal the quality (i.e. accuracy) by which the topographic surface functions are represented in the spherical harmonic domain through the GLQ quadrature (section 4.3.2, 4.3.3 and 4.3.4), and may be interpreted as truncation errors 4.4.1.
By performing another harmonic analysis and synthesis using band-limited topographic input grids of the three planets (obtained by synthesis using the SHCs from the initial SHA), we can investigate the precision of the GLQ quadrature in closed loop manner (similar to the experiments done for the DH and the GLQ algorithm in section 3.2 up to degree 21600). The results - space domain residual errors - are shown in the bottom plot of figure 6, 10 and 12. The absolute amplitudes of the errors (Earth: < 3 mm; Mars: < 0.03 mm; Moon: < 1 mm) suggest that the GLQ algorithm works very precise even at the ultra-high harmonic degrees and that the precision is not the limiting factor for the application of the algorithm to planetary topography in this work.
All residual plots from band-limited input topography reveal a striping pattern along latitude parallels, which is interrupted by white areas (indicating less or no errors) that show some obvious correlation to the topography. Similar striping patterns can be investigated for using the DH algorithm instead (not shown here). This striping is entirely non-critical for the application to digital elevation data of the planetary topography done here, nevertheless it deserves some close-up investigation. In case of Earth, this pattern can be characterized as follows: ocean and continental areas of about ± 2000 m elevation are free of the striping pattern; higher or lower elevated areas are affected by the striping. Thus, the floor of the large oceans (except for the ridges), the Himalayas, but also Olympus Mons on Mars are covered by striping. Due to the strict east-west alignment of the striping pattern, the error must originate from the zonal harmonic coefficients. Those are, e.g., dependent on the Legendre Polynomials (LPs). However, the LPs are determined accurately using exact identities (see section 3.1). Nevertheless, at very high or very low elevated points the algorithm must be at the edge of arithmetic over/-underflow, setting the limits for the precision of the quadrature and leading to the characteristic error patterns in the spatial domain. This may be an issue for extremely high-resolution quadratures (e.g. up to some hundred thousands of degrees) some day in the future.

5 SUMMARY AND OUTLOOK

In this work, two known algorithms - the Gauss-Legendre quadrature and the quadrature following Driscoll/Healy - and their implementation for the purpose of ultra-high (surface) spherical har-

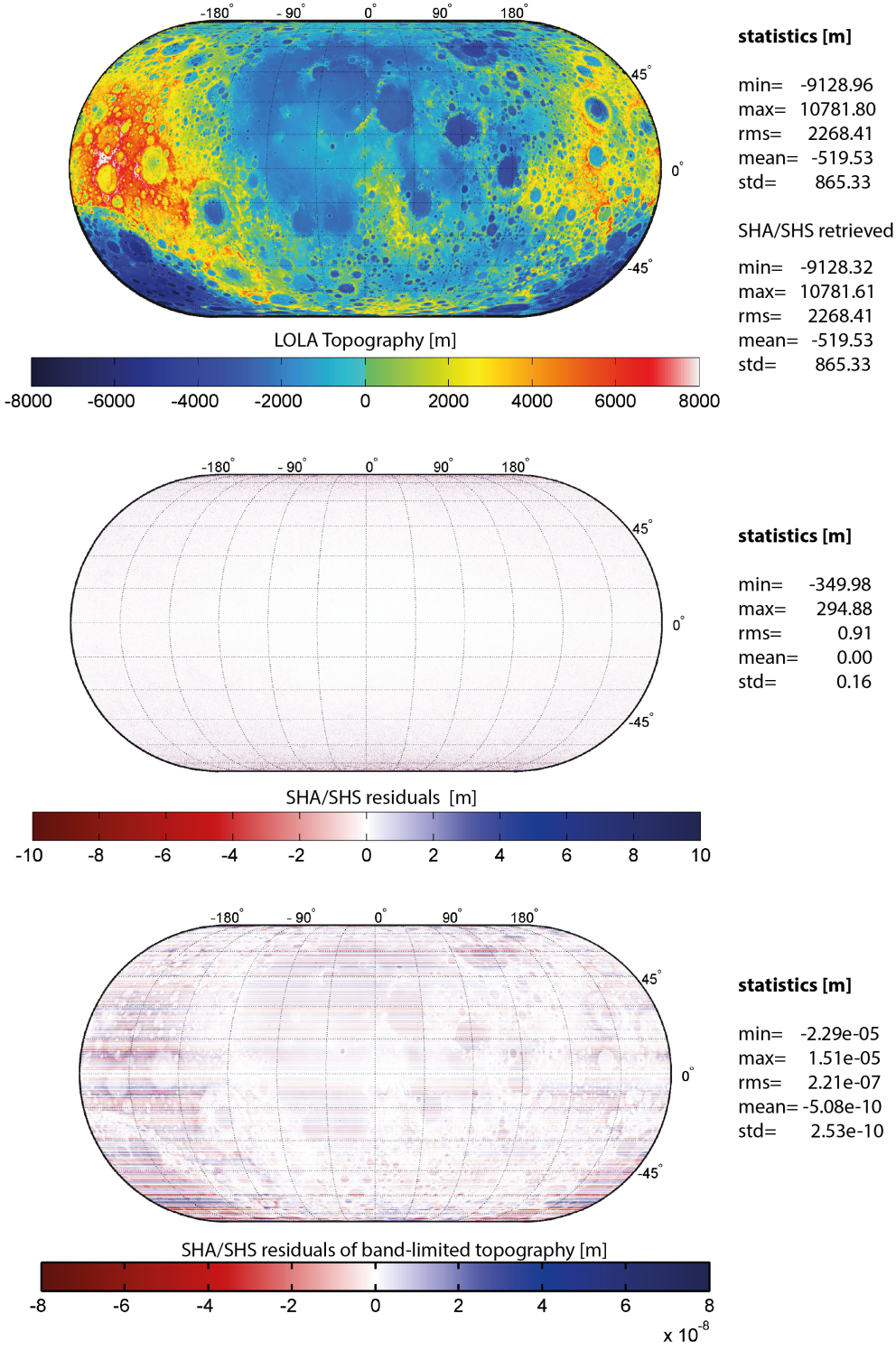

Fig. 12 Lunar topography (upper plot), closed loop residuals with input topography after the first spherical harmonic analysis and synthesis (middle plot) and residuals of the anaylsis and synthesis of a band-limited input topography (to degree 46080); unit is metres.

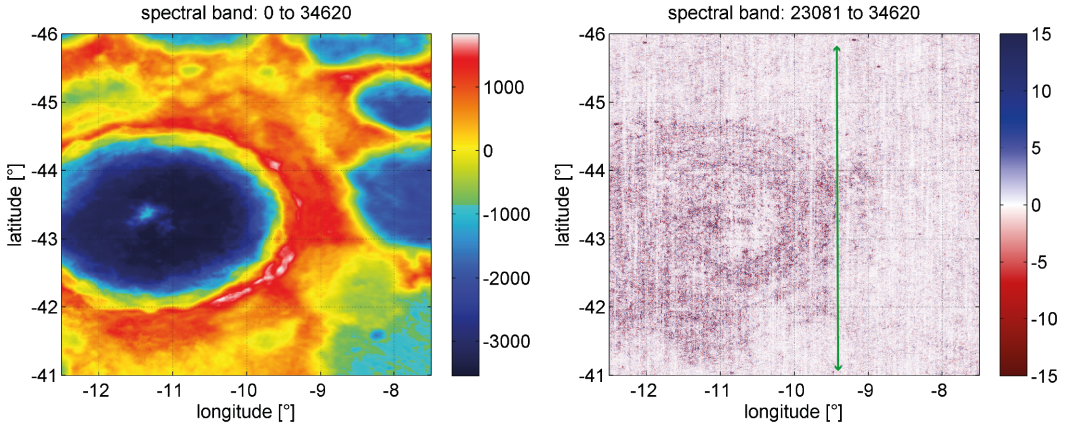

Fig. 13 Elevations around Tycho crater obtained from a analysis and synthesis of LOLA data in the spectral band 0...34620 (left) and 23081...34620 (right); the green arrows indicate the direction of the visible striping pattern; unit is metres.

monic analysis of spheroid functions were presented in detail. We extended the implementation of the algorithms found in the SHTOOLS software package by 1) the X-number (or Extended Range Arithmetic) method for accurate computation of ALFs and 2) OpenMP directives enabling parallel computing for feasible computation times. A degree 21600 quadrature (of a degree 21600 band-limited topographic function) that involves the computation of over 466×10^6 parameters, shows a precision of at least 3×10^{-5} m and 5×10^{-5} m in the space domain for the GL and DH algorithm, respectively. Sharing the degree-21600 quadrature between 8 or 14 CPUs, the computation times could be reduced approximately to a sixth (to ~ 12.1 h) or a thirteenth (to ~ 5.9 h) of the single-thread time in case of the GL algorithm and to a fifth (to ~ 49.5 h) or thirteenth (to ~ 16.9 h) of the single-thread time in case of the DH algorithm. Hence, the Gauss-Legendre algorithm can be considered computationally more effective, although neither algorithm is inferior in terms of numerical precision.

The implementation of the GL-quadrature was then used to harmonically analyse the Earth's topography and bathymetry (from the SRTM15 PLUS data set) to degree 43200, the Martian topography (from MOLA data products) to degree 23040 and the Lunar topography (from LOLA data products) to degree 46080. The retrieved spherical harmonic coefficients gave spectral insights into the different short and ultra-short wavelength characteristics of the topography of the three bodies. Degree variances reveal that the power (variability) of the Moon's topography is significantly larger compared to the planets at all spatial scales (at least down to a half-wavelength of 500 m), especially below scales of 200 km. The representation of the Earth's bathymetry (only) and topography (only) in terms of degree variances reveal irregularities in the bathymetry data of SRTM15 PLUS data set. The bathymetric degree variance curve exhibits a change in the decay of the spectral power around degree 2160, which indicates the limit of full resolution in contemporary bathymetry data, based on inversion of gravity from satellite altimetry. Neglecting these irregularities, we find the ocean floors making up most of the Earth's topographic variability at scales above 5 km and the continental topography making up most power below scales of 5 km ($\sim$ degree 4000) .

Importantly, the residuals and the ultra-high bands of the spectral representation may also be used to reveal artifacts and systematics/characteristics of the observation techniques used for the creation of the elevation data. In case of SRTM15 PLUS, ship-tracks become clearly visible in the bathymetry and an artifact over Antarctica and the Arctic ocean was detected. In case of MOLA and LOLA, the synthesis of certain spectral bands (e.g. 2160 to 10800) reveals the ground tracks of the orbiters that carried the laser altimeters.

The accuracy of the representation of the planets' topography in spherical harmonics was investigated in terms of residual errors in the space domain. The global STD of the residuals are 3.06 m for Earth (d/o 43200), 1.94 m for Mars and 0.91 m for Moon. Apart from the rather high residuals in case of Earth, the results corroborate that choosing a higher degree in the analysis minimizes the truncation error. Among others, artifacts and ship-track edges in the SRTM15 PLUS data set

might be responsible for comparatively high residuals in the case of Earth. The residuals in all cases generally show a high correlation with the topography and most errors are found over areas of steep (or rough) terrain (e.g. mountains, trenches, crater edges). Investigation of the quadrature precision for the three cases of high-degree spherical harmonic analysis in closed loop manner shows east-west aligned stripes (caused by the zonal coefficients) which are pronounced in high and low elevated areas at the $1\text{x}10^{-7}$ m level, with the absolute errors not exceeding 3 mm for Earth, 0.03 mm for Mars and 1 mm for the Moon.

As the key conclusion, both algorithms and their implementation are suitable for efficient and accurate ultra-high degree spherical harmonic analysis of spheroidal functions, tested here up to degree 46080. The Gauss-Legendre algorithm outperforms the Driscoll/Healy algorithm in terms of computation times and therefore is preferable.

The extension of the algorithms for solid spherical harmonic analysis (e.g. of a functional of the gravitational field) is possible and would certainly extend the applicability of the algorithms in geophysics and geodesy.

Acknowledgements This study was supported by the Australian Research Council (Grant DP12044100) and through funding from Curtin University's Office of Research and Development. Further, it was created with the support of the Technische Universität München - Institute for Advanced Study, funded by the German Excellence Initiative. We gratefully acknowledge the thorough work of Mark Wieczoreck who developed SHTOOLS in the first place and distributes the code freely to the community. We also want to thank all the colleagues who were involved in the construction or contributed to any of the planetary topography data sets used in this work.

References

Abrykosov O, Förste C, Gruber C, Shako R, Barthelmes F (2012) Harmonic analysis of the DTU10 global gravity anomalies. In: Abbasi A, Giesen N (eds) EGU General Assembly Conference Abstracts, EGU General Assembly Conference Abstracts, vol 14, p 4945

Andersen O, Knudsen P, Kenyon S, Factor J, Holmes S (2013) The dtu13 global marine gravity field - first evaluation. Tech. rep., DTU Space - National Space Institute

Arabelos D, Tscherning C (1998) The use of least squares collocation method in global gravity field modeling. Physics and Chemistry of the Earth 23(1):1 – 12, DOI http://dx.doi.org/10.1016/S0079-1946(97)00234-6, URL http://www.sciencedirect.com/science/article/pii/S0079194697002346

Balmino G, Vales N, Bonvalot S, Briais A (2012) Spherical harmonic modelling to ultra-high degree of bouguer and isostatic anomalies. Journal of Geodesy 86(7):499–520, DOI 10.1007/s00190-011-0533-4, URL http://dx.doi.org/10.1007/s00190-011-0533-4

Bartusch M, Berg H, Siebertz O (2008) The TanDEM-X Mission. In: Synthetic Aperture Radar (EUSAR), 2008 7th European Conference on, pp 1–4

Becker J, Sandwell D, Smith W, Braud J, Binder B, Depner J, Fabre D, Factor J, Ingalls S, Kim SH, Ladner R, Marks K, Nelson S, Pharaoh A, Trimmer R, Von Rosenberg J, Wallace G, Weatherall P (2009) Global bathymetry and elevation data at 30 arc seconds resolution: Srtm30_plus. Marine Geodesy 32(4):355–371, DOI 10.1080/01490410903297766, URL http://dx.doi.org/10.1080/01490410903297766, http://dx.doi.org/10.1080/01490410903297766

Bucha B, Janák J (2013) A MATLAB-based graphical user interface program for computing functionals of the geopotential up to ultra-high degrees and orders. Computers Geosciences 56:186–196

Claessens S (2006) Solutions to Ellipsoidal Boundary Value Problems for Gravity Field Modelling. PhD thesis, Curtin University of Technology

Claessens S, Hirt C (2013) Ellipsoidal topographic potential - new solutions for spectral forward gravity modelling of topography with respect to a reference ellipsoid. Journal of Geophysical Research 118(11):5991–6002, DOI 10.1002/2013JB010457

Colombo O (1981) Numerical methods for harmonic analysis on the sphere. Tech. Rep. Rep. No. 310, The Ohio State University

Dassios G (2012) Ellipsoidal Harmonics. Cambridge University Press, URL http://dx.doi.org/10.1017/CBO9781139017749

Driscoll J, Healy D (1994) Computing Fourier Transforms and Convolutions on the 2-Sphere. Advances in Applied Mathematics 15(2):202–250, DOI 10.1006/aama.1994.1008

ESA (1999) Gravity Field and Steady-State Ocean Circulation Mission. Report for the mission selection of the four candiate earth explorer missions (ESA SP-1233(1)), European Space Agency

Farr T, Rosen P, Caro E, Crippen R, Duren R, Hensley S, Kobrick M, Paller M, Rodriguez E, Roth L, Seal D, Shaffer S, Shimada K, Umland J, Werner M, Oskin M, Burbank D, Alsdorf D (2007) The Shuttle Radar Topography Mission. Reviews of Geophysics 45(RG2004), DOI 10.1029/2005RG000183

Fecher T, Pail R, Gruber T (2013) Global gravity field modeling based on goce and complementary gravity data. International Journal of Applied Earth Observation and Geoinformation DOI 10.1016/j.jag.2013.10.005

Fukushima T (2012) Numerical computation of spherical harmonics of arbitrary degree and order by extending exponent of floating point numbers. Journal of Geodesy 86(4):271–285, DOI 10.1007/s00190-011-0519-2, URL http://dx.doi.org/10.1007/s00190-011-0519-2

Gruber C (2011) A study on the fourier composition of the associated legendre functions; suitable for applications in ultra-high resolution. Scientific technical report 11/04, German Research Centre for Geosciences (GFZ), Potsdam, Germany, DOI 10.2312/GFZ.b103-11041

Gruber C, Novak P, Sebera J (2011) FFT-based high-performance spherical harmonic transformation. Studia Geophysica et Geodaetica 55:489–500

Gruber C, Barthelmes F, Flechtner F, Novak P (2014) Derivation of Topographic potential from global DEM Models. In: Rizos C, Willis P (eds) Earth on the Edge : Science for a Sustainable Planet : Proceedings of the IAG General Assembly, Melbourne, Australia, June 28 - July 2, 2011, Berlin : Springer, vol 139, pp 535 – 542

Hirt C, Kuhn M (2014) A band-limited topographic mass distribution generates a full-spectrum gravity field - gravity forward modelling in the spectral and spatial domain revisited. Journal of Geophysical Research - Solid Earth 119, DOI doi:10.1002/2013JB010900

Hirt C, Rexer M (2015) Earth2014: 1' shape, topography, bedrock and ice-sheet models - available as gridded data and degree 10,800 spherical harmonics. International Journal of Applied Earth Observation and Geoinformation DOI 10.1016/j.jag.2015.03.001

Hofsommer D (1957) On the expansion of a function in a series of spherical harmonics. Tech. Rep. Rep. No. R344A, Computation Department of the Mathematical Centre, Amsterdam

Hofsommer D, Potters M (1960) Table of fourier coefficients of associated legendre functions. Report r 478. knaw, Computational Department of the Mathematical Centre, Amsterdam, The Netherlands

Holmes S, Featherstone W (2002) A unified approach to the Clenshaw summation and the recursive computation of very high degree and order normalised associated Legendre functions. Journal of Geodesy 76:279–299, DOI 10.1007/s00190-002-0216-2

Krylov V (1962) Approximate Calculation of Integrals. MacMillan, New York

Lemoine F, Smith DE, Rowlands D, Zuber M, Neumann G, Chinn D, Pavlis D (2001) An improved solution of the gravity field of Mars (GMM-2B) from Mars Global Surveyor. Journal of Geophysical Research 106:23,359Ű23,376

Lemoine FG, Goossens S, Sabaka TJ, Nicholas JB, Mazarico E, Rowlands DD, Loomis BD, Chinn DS, Neumann GA, Smith DE, et al (2014) Grgm900c: A degree 900 lunar gravity model from grail primary and extended mission data. Geophysical Research Letters 41(10):3382–3389

Marks K, Smith W, Sandwell D (2010) Evolution of errors in the altimetric bathymetry model used by google earth and gebco. Marine Geophysical Researches 31(3):223–238

Moritz H (1978) Least-squares collocation. Reviews of Geophysics 16(3):421–430, DOI 10.1029/RG016i003p00421, URL http://dx.doi.org/10.1029/RG016i003p00421

Moritz H (2000) Geodetic Reference System 1980. Journal of Geodesy 74(1):128–162, DOI 10.1007/s001900050278

Neumann G (2010) 2009 lunar orbiter laser altimeter raw data set, lro-l-lola-4-gdr-v1.0, pds. Tech. rep., NASA

Pail R, Goiginger H, Schuh W, Höck E, Brockmann J, Fecher T, Mayer-Gürr T, Kusche J, Jäggi A, Rieser D, Gruber T (2011) Combination of GOCE data with complementary gravity field information (GOCO). In: Proceedings of 4th International GOCE User Workshop, Munich, 31st

March 2011
Rummel R, Rapp R, Sünkel H, Tscherning C (1988) Comparisons of Global Topographic/Isostatic Models To the Earth's Observed Gravity Field. OSU report 388, Ohio State University
Sandwell DT, Müller RD, Smith WH, Garcia E, Francis R (2014) New global marine gravity model from cryosat-2 and jason-1 reveals buried tectonic structure. science 346(6205):65–67
Smith DE, Zuber M, Neumann G, Guinness E, Slavney S (2003) Mars global surveyor laser altimeter mission experiment gridded data record (mgs-m-mola-5-megdr-l3-v1.0). Tech. rep., NASA Planetary Data System
Smith DE, Zuber M, Jackson G, Cavanaugh J, Neumann G, Riris H, Sun X, Zellar R, Coltharp C, Connelly J, Katz R, Kleyner I, Liiva P, Matuszeski A, Mazarico E, McGarry J, Novo-Gradac AM, Ott M, Peters C, Ramos-Izquierdo L, Ramsey L, Rowlands D, Schmidt S, Scott I VStanley, Shaw G, Smith J, Swinski JP, Torrence M, Unger G, Yu A, Zagwodzki T (2010) The Lunar Orbiter Laser Altimeter Investigation onătheăLunar Reconnaissance Orbiter Mission. Space Science Reviews 150(1-4):209–241, DOI 10.1007/s11214-009-9512-y, URL http://dx.doi.org/10.1007/s11214-009-9512-y
Smith WH, Sandwell DT (1994) Bathymetric prediction from dense satellite altimetry and sparse shipboard bathymetry. Journal of Geophysical Research: Solid Earth (1978–2012) 99(B11):21,803–21,824
Sneeuw N (1994) Global spherical harmonic analysis by least-squares and numerical quadrature methods in historical perspective. Gepohysical Journal International 118:707–716
Tachikawa T, Hato M, Kaku M, Iwasaki A (2011) Characteristics of ASTER GDEM version 2. In: Geoscience and Remote Sensing Symposium (IGARSS), 2011 IEEE International, IEEE, pp 3657–3660
Torge W (2001) Geodesy, 3rd edn. Walter de Gruyter
Walker JS (1996) Fast fourier transforms, vol 24. CRC press
Wieczorek M (2007) The gravity and topography of the terrestrial planets. Treatise on Geophysics 10:165–206, DOI 10.1016/B978-044452748-6/00156-5
Wieczorek M (2015) 10.05 - gravity and topography of the terrestrial planets. In: Schubert G (ed) Treatise on Geophysics (Second Edition), second edition edn, Elsevier, Oxford, pp 153 – 193, DOI http://dx.doi.org/10.1016/B978-0-444-53802-4.00169-X, URL http://www.sciencedirect.com/science/article/pii/B978044453802400169X
Wood C, Anderson L (1978) New morphometric data for fresh lunar craters. In: Lunar and Planetary Science Conference Proceedings, vol 9, pp 3669–3689